Upstream Subtropical Signals Preceding the Asian Summer Monsoon Circulation

Song Yang

Climate Prediction Center, NOAA/NWS/NCEP, Camp Springs, Maryland

K.-M. Lau

NASA GSFC Laboratory for Atmospheres, Greenbelt, Maryland

S.-H. Yoo

School of Earth and Environmental Sciences, Seoul National University, Seoul, South Korea

J. L. Kinter and K. Miyakoda

Center for Ocean–Land–Atmosphere Studies, Calverton, Maryland

C.-H. Ho

School of Earth and Environmental Sciences, Seoul National University, Seoul, South Korea

(Manuscript received 9 July 2003, in final form 19 May 2004)

ABSTRACT

In this study, the authors address several issues with respect to the antecedent signals of the large-scale Asian summer monsoon that were earlier identified by Webster and Yang. In particular, they revisit the changes in the subtropical upper-tropospheric westerlies preceding the monsoon, depict the detailed structure of the monsoon's antecedent signals, and investigate the physical processes from the signals to the monsoon. They also explore the teleconnection of these signals to various large-scale climate phenomena and emphasize the importance of the upstream location of the signals relative to the Tibetan Plateau and the monsoon.

Before a strong (weak) Asian summer monsoon, the 200-mb westerlies over subtropical Asia are weak (strong) during the previous winter and spring. A significant feature of these signals is represented by the variability of the Middle East jet stream whose changes are linked to the Arctic Oscillation, North Atlantic Oscillation, El Niño–Southern Oscillation, and other climate phenomena. When this jet stream intensifies and shifts southeastward, cold air intrudes frequently from eastern Europe into the Middle East and southwestern Asia. As a result, in subtropical Asia, snow and precipitation increase, the ground wetness increases, and surface temperature decreases. A strengthening Middle East jet stream is also accompanied by increases in both stationary wave activity flux and higher-frequency eddy activities. The Tibetan Plateau acts to block these westerly activities propagating eastward and increase the persistence of the low-temperature anomalies, which in turn prolongs the atmospheric signals from winter to spring.

A strong link is found between the persistent low-temperature anomalies and the decrease in geopotential height over southern Asia, including the Tibetan Plateau, in spring. The latter indicates a late establishment of the South Asian high, and implies a delay in the atmospheric transition from winter to summer conditions and in the development of the summer monsoon. The preceding scenario for a strong Middle East jet stream and a weaker Asian monsoon can be applied accordingly for the discussion of the physical processes from a weak jet stream to a strong monsoon.

The current results of the relationship between the extratropical process and Asian monsoon resemble several features of the tropical–extratropical interaction mechanism for the tropospheric biennial oscillation (TBO). While the role of tropical heating is emphasized in the TBO mechanism, compared to the variability of the sea surface temperature related to El Niño–Southern Oscillation, the extratropical process examined in this study is more strongly linked to the Asian summer monsoon.

Corresponding author address: Dr. Song Yang, Climate Prediction Center, NCEP/NWS/NOAA, 5200 Auth Road, Rm 605, Camp Springs, MD 20746.
E-mail: song.yang@noaa.gov

1. Introduction

The relationship between the large-scale Asian summer monsoon (hereafter ASM) and El Niño–Southern Oscillation (ENSO) has been studied for many decades, especially since the occurrence of the 1982/83 ENSO event. One of the dilemmas in studying this relationship is that, although the ASM is more strongly related to the ENSO phenomena after the monsoon season than those before the monsoon season, ENSO has more often been considered an important predictor for the monsoon than vice versa. In fact, the stronger relationship between monsoon and the ENSO events that follow the monsoon season was noticed by Walker several decades ago (e.g., Walker 1923, 1924) for the Indian monsoon component and the Southern Oscillation. This feature led Normand (1953) to state that "the Indian monsoon therefore stands out as an active, not a passive feature in world weather, more efficient as a broadcasting tool than as an event to be forecast." The behavior of this monsoon–ENSO relationship during the recent decades can be depicted, as shown in Fig. 1, by computing the lag correlation between the monthly Niño-3 (5°S–5°N, 150°–90°W) sea surface temperature (SST) and the all-India summer monsoon rainfall. Figure 1, which shows a feature similar to that discussed by Shukla and Paolino (1983; see their Fig. 2), indicates that the simultaneous relationship and the monsoon-lead correlation are much stronger than the correlation in which the SST anomaly leads the monsoon.

The preceding discussion implies that further studies are needed to demonstrate the importance of the ASM for ENSO prediction and to seek other antecedent signals that can be considered potential predictors for the monsoon. Such antecedent signals may or may not be associated directly with ENSO, but they must be linked to slowly varying forcing or large-scale atmospheric patterns of different forms. Webster and Yang (1992) have discussed the requirements in time and spatial scales and the cause-and-effect aspect for a signal to be considered a precursor of the monsoon. Perhaps there exist many of these signals, but only few of them have been explored. On interannual time scales, extensive
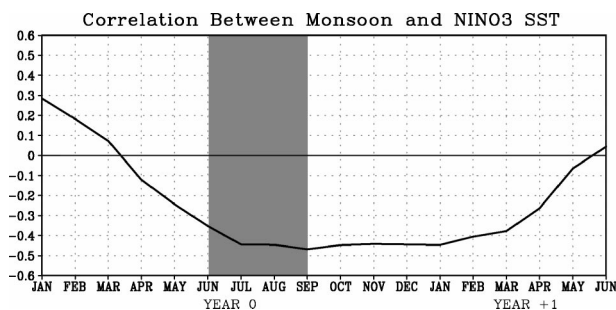

Fig. 1. Lag correlation between all-India monsoon rainfall (from Jun to Sep) and monthly Niño-3 (5°S–5°N, 150°–90°W) sea surface temperature for the period of 1968–2001. The months of summer monsoon are highlighted.

studies have followed Walker (1923, 1924) and Blanford (1884) to focus on ENSO (e.g., Rasmusson and Carpenter 1982; Ropelewski and Halpert 1987; Webster and Yang 1992; Zhang et al. 1996; Soman and Slingo 1997; Tao and Zhang 1998; Miyakoda et al. 1999; Navarra et al. 1999; Lau and Nath 2000; Slingo and Annamalai 2000; Wang et al. 2000; Wang and Li 2004) and the land surface process of the Eurasian continent, including the Tibetan Plateau (Hahn and Shukla 1976; Murakami and Ding 1982; Luo and Yanai 1984; He et al. 1987; Barnett et al. 1989; Yanai et al. 1992; Meehl 1994; Lau and Bua 1998; Webster et al. 1998; Yang and Lau 1998; Bamzai and Shukla 1999). Others have examined the precursory features associated with low-frequency atmospheric circulation (Murakami et al. 1986; Webster and Yang 1992) and the monsoon's annual migration (Meehl 1987; Yasunari 1991; Zeng and Zhang 1998; Annamalai et al. 1999; LinHo and Wang 2002). In particular, for the Indian monsoon, several studies have connected the monsoon to the antecedent changes in the tropical and extratropical trough and ridge systems, and found that one of the leading indicators for predicting the variability of the Indian monsoon is the location of the 500-mb ridge along 75°E (Ramaswamy 1962; Banerjee et al. 1978; Thapliyal 1982; Mooley et al. 1986). When the ridge, whose location measures the influence of westerly troughs on the thermal conditions over northern India, is located farther south than normal, northern and central India is frequently influenced by westerly disturbances and cold air intrusions from higher latitudes. This condition favors a delayed and weaker monsoon in the following summer.

It should be pointed out that, within the earlier-discussed scope, several studies have described similar features in the context of tropospheric biennial oscillation (TBO), in which tropical–extratropical interaction is emphasized (Yasunari and Seki 1992; Meehl 1994, 1997; Ogasawara et al. 1999; Meehl and Arblaster 2002a,b). As summarized by Meelh and Arblaster (2002a; see their Fig. 3), in December–January–February (DJF) of warm SST in the Indian and central eastern Pacific Oceans and cold SST to the north of Australia (associated with weak Australian monsoon), the Rossby wave response to the tropical heating causes less snow and warmer conditions over the Eurasian continent. In the following March–April–May (MAM), many of the earlier signals in the coupled ocean–atmosphere–land system persist because of the memories in SST and the associated thermocline conditions. As a consequence, the Asian summer monsoon is strong. In the meantime, the Eurasian land surface cools because of the heavy rainfall, and SST decreases in the Indian and central Pacific Oceans and increases in the western Pacific. The earlier-mentioned summertime conditions, maintained to September–October–November (SON) owing to the strong zonal cells and coupled wind–ocean response from the previous seasons, lead to strong Australian monsoon in the next DJF. As a Rossby wave
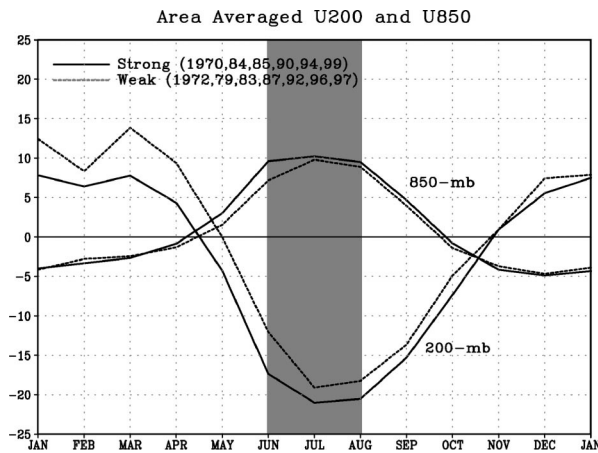
FIG. 2. Monthly values of zonal winds (m s^{-1}) at 200- and 850-mb levels for strong ASM (solid lines; 1970, 1984, 1985, 1990, 1994, and 1999) and weak ASM (dashed lines; 1972, 1979, 1983, 1987, 1992, 1996, and 1997). The composite values are averaged within 5°–20°N, 40°–110°E, and computed with respect to the intensity of WY monsoon index in JJA, which is highlighted.

response, the strong convection of the Australian monsoon and weak convection over the western Indian Ocean and central Pacific cause an anomalous trough and cold temperature over Eurasia, followed by weak South Asian summer monsoon.

It is possible that even a decent antecedent signal may not be a strong predictor for the monsoon. However, it should at least possess a potential for monsoon prediction. Also, even though many precursors have been sought and some of them have been believed to possess a cause-and-effect significance, the mechanisms responsible for the precursor–monsoon relationship often remain overly complicated. Thus, it is always preferable if the physical processes from the precursors to the monsoon can be revealed and explained clearly by a sound scenario.

This current study addresses the antecedent signals of the large-scale ASM that occur in the subtropics and extratropics during winter and spring seasons. Webster and Yang (1992) found that the upper-tropospheric westerlies over subtropical Asia are stronger (weaker) than normal in the winter and spring seasons before weak (strong) ASM circulation. This relationship between the monsoon and the antecedent signals is summarized in Fig. 2, which shows monthly, area-averaged zonal winds at 200- and 850-mb levels. The composite values are computed with respect to the strong and weak summer monsoons measured by the Webster–Yang (WY) monsoon index (see Webster and Yang 1992), which is defined as the difference in zonal wind between 850 and 200 mb averaged over the area of 0°–20°N, 40°–110°E. The 200-mb zonal wind (U200) in winter and spring is stronger before a weak monsoon. On the contrary, the zonal wind is weaker before a strong monsoon. However, this relationship is less obvious in the 850-mb

wind, which is usually out of phase with the 200-mb component.

Ju and Slingo (1995) and Yang et al. (1996) have found that this feature can be reproduced by atmospheric general circulation models forced by globally varying SST. The remote effect of tropical SST, especially the ENSO-related SST, has been speculated as a cause of the antecedent signals of the monsoon (Webster and Yang 1992; Ju and Slingo 1995; Yang et al. 1996; Thomas et al. 2000; Miyakoda et al. 2003). However, Yang et al. (1996) and Yang and Lau (1998) have demonstrated that the signals are also connected to the land surface process (e.g., changes in soil moisture content and snow amount) over the Eurasian continent. Kawamura (1998) and Shen et al. (1998) have also provided evidence about the importance of the precursory atmospheric anomalies over the Eurasian continent for the ASM. Furthermore, Yasunari and Seki (1992), Dugam et al. (1997), Chang et al. (2001), and Gong and Ho (2003) have discussed the possible connection of ASM to the North Atlantic Oscillation (NAO) and the Arctic Oscillation (AO). This suggests the need to examine the role of these large-scale climate phenomena in the appearance of the monsoon's antecedent signals, which will also be addressed in the current study.

In this analysis, we first revisit the earlier signal–monsoon relationship using updated observations with the goal of improving the understanding of several important aspects of this relationship. We will depict the detailed structure of the antecedent signals, reveal the physical processes connecting these signals to the monsoon, and explore the teleconnection of the signals to larger-scale circulation features. While some features of the extratropical signals and ASM have been explained previously in the context of TBO (e.g., Meehl and Arblaster 2002a), we focus on the detailed physical process (especially those associated with the Middle East jet stream) in a wider range of time scales and the relative importance of the extratropical versus ENSO signals for the variability of ASM. We refer to the antecedent signals, or precursory signals used alternatively, as *the signals.* Unless specified, the monsoon discussed in this paper refers to the large-scale ASM measured by the WY index.

The rest of this paper is organized as follows. In the next section, we describe briefly the datasets that are used in the analysis. In section 3, we display the antecedent signals of the ASM using updated information. A better understanding of the signals and the physical process linking them to the monsoon is given in section 4. The discussion in section 5 will be aimed at the teleconnection of the antecedent signals with AO, NAO, ENSO, and other large-scale climate features occurring before the monsoon. Finally, we summarize our results in section 6.

2. Data

The principal dataset applied in this study is the commonly used atmospheric reanalysis produced by the Na-

tional Centers for Environmental Prediction (NCEP) and the National Center for Atmospheric Research (Kalnay et al. 1996). We analyze the winds, geopotential height, and temperature from the reanalysis product. Because of the potential problems with using the early portion of this dataset for studying the Asian monsoon (Yang et al. 2002), we use only the data after 1967 (from January 1968 to March 2004). We also analyze the surface air temperatures (T_s) from the Global Telecommunication System (GTS) and the Goddard Institute for Space Studies (GISS; of the National Aeronautics and Space Administration). The GTS T_s, provided by Dr. P. Xie at the NCEP Climate Prediction Center (CPC), is available daily, covering the period from 1979 to the present. The GISS T_s comes from surface temperature analysis (Peterson and Vose 1997; Hansen et al. 1999). Details of the GISS analysis can be found online at http://www.giss.nasa.gov/data/update/gistemp.

The other data analyzed in this study include the all-India monsoon rainfall (e.g., Parthasarathy et al. 1991), the National Oceanic and Atmospheric Administration (NOAA) reconstructed SST (Smith and Reynolds 2003), the precipitation analysis of the Climatic Research Unit (CRU) of the University of East Anglia (New et al. 1999, 2000), and NOAA snow cover data (starting from 1972; http://www.cpc.ncep.noaa.gov/data/snow). Although covering different time periods, all these are well-established datasets, which have been applied widely in climate studies.

3. Antecedent signals of the Asian monsoon

Figure 3 shows the composite patterns of the difference in U200 between strong and weak ASM for December–February, March–May, and June–July–August (JJA). They are constructed based on the intensity of monsoon in JJA, and the summers of strong (weak) monsoon measured by the WY index are selected as those when the monsoon is stronger (weaker) than normal by one standard deviation or more. Figure 3a (DJF) and Fig. 3b (MAM) use the same sample of the JJA (Fig. 3c) as the reference of the summer monsoon. In other words, Figs. 3a and 3b are, respectively, 4–6 and 1–3 months earlier than Fig. 3c (JJA). The figure indicates that the upper-tropospheric westerlies over subtropical Asia are stronger (weaker) in the winter and spring seasons before weak (strong) ASM. Figure 3a (DJF) shows a wave train–like structure near the Middle East and over East Asia, which will be discussed in detail shortly (see discussion for Fig. 5a). In Fig. 3b (MAM), the features associated with strong ASM include not only a decrease in westerlies over the northern Arabian Sea and India but also an increase in westerlies to the north. As will be seen later (e.g., Fig. 10), these changes represent anomalous circulation features over the Tibetan Plateau and adjacent regions that will be occupied in summer by the South Asian high, which plays a critical role in the development of ASM.
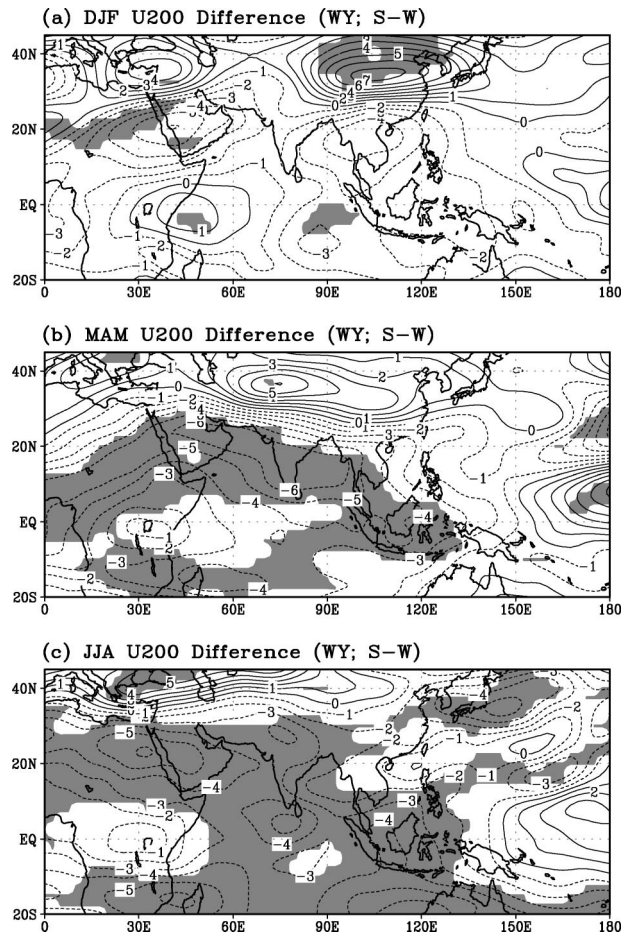

FIG. 3. Differences in U200 (m s^{-1}) between strong and weak ASM (see Fig. 2) for (a) previous DJF (b) previous MAM, and (c) JJA. The patterns are constructed with respect to the intensity of WY index in JJA. Values exceeding significantly the 90% confidence level are shaded.

Although the patterns shown in Fig. 3 are constructed based on the intensity of ASM in JJA, they are all very similar to the most dominant modes of the regional atmospheric circulation in respective seasons. Figure 4 shows the first-mode patterns of the empirical orthogonal function (EOF) analysis of U200 for DJF, MAM, and JJA, respectively. The EOF analysis shares many major features shown in Fig. 3 such as those over the Middle East and East Asia in DJF, those over the tropical–subtropical Asia in MAM, and the variations of ASM in JJA. Especially, for DJF, the correlation between the first principal component (PC) and an index measuring the Middle East jet stream (see Fig. 5b shortly) is −0.42. For MAM, the correlation between the PC and an index measuring the geopotential height in the location of the summer South Asian high (see Fig. 10 later) is 0.35. Finally, for JJA, the correlation between the PC and the ASM is 0.67. These correlation coefficients are all significant and exceed the 95% confidence level (for the period of 1968–2004). These features dem-

First EOF Modes of U200

(a) DJF (26.31%)

(b) MAM (25.27%)

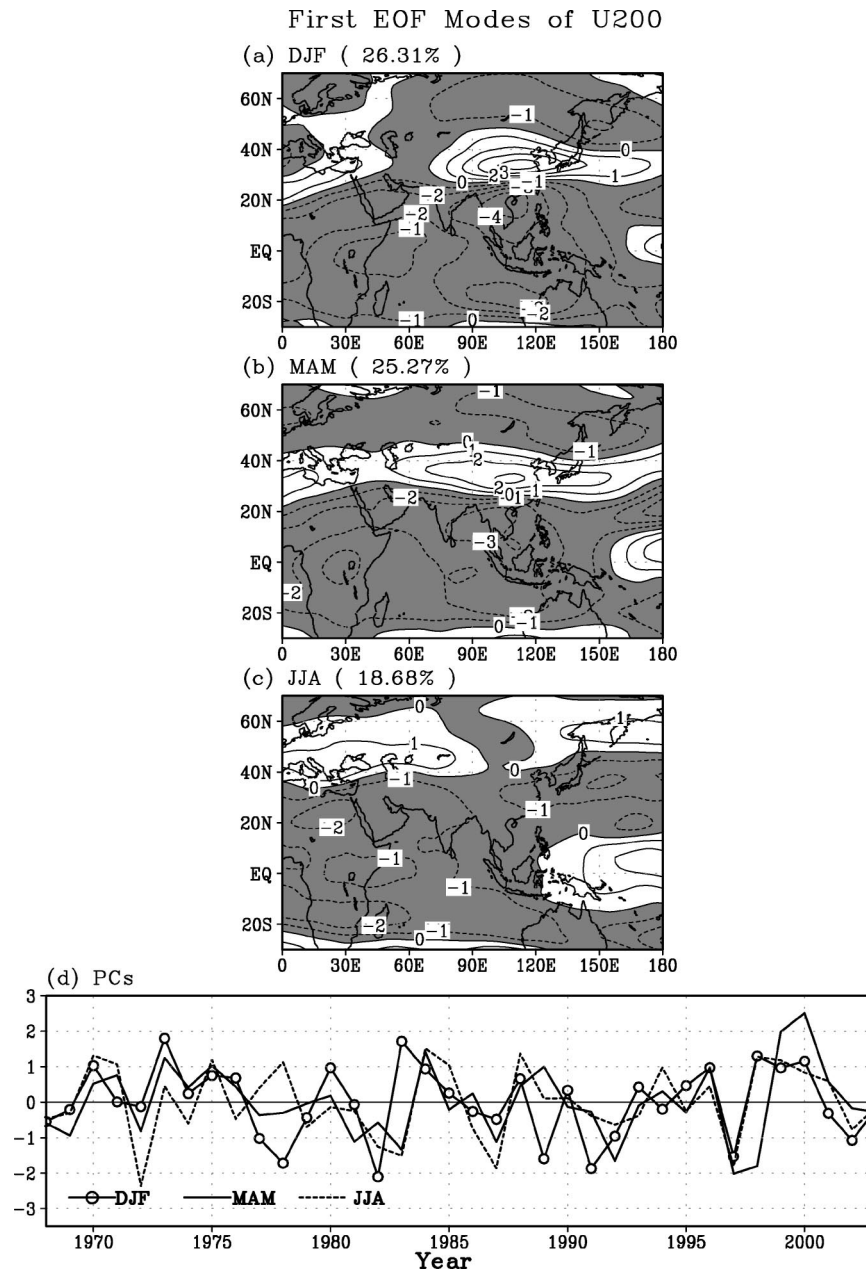(c) JJA (18.68%)

(d) PCs

FIG. 4. First modes of the empirical orthogonal function analysis of U200 for (a) DJF, (b) MAM, and (c) JJA. (d) The principal components corresponding to the EOF modes of various seasons where year 1970 refers to DJF 1969/70, MAM 1970, and JJA 1970, correspondingly. Negative values are shaded.

onstrate the robustness of the monsoon's antecedent signals and their relationship with the summer monsoon.

We now explore other features of the ASM-related antecedent changes in U200. Several salient features emerge from Fig. 5a, which shows the difference in DJF U200 between strong and weak ASM in a domain much larger than that shown in Fig. 3a. First, over the eastern Pacific, a wave train emanates from the equator and extends into North America. [The pattern of geopoten-

tial height (not shown), which is more appropriate to portray atmospheric wave trains, reveals similar features to Fig. 5a.] This feature mimics the ENSO-related change in atmospheric circulation and thus indicates a link between the large-scale ASM and ENSO (also see Table 1 later). Second, in East Asia, an increase in westerlies appears over 40°–50°N. Such an increase is associated with decreases in the winds to the north and south, and is linked to changes in the westerlies over

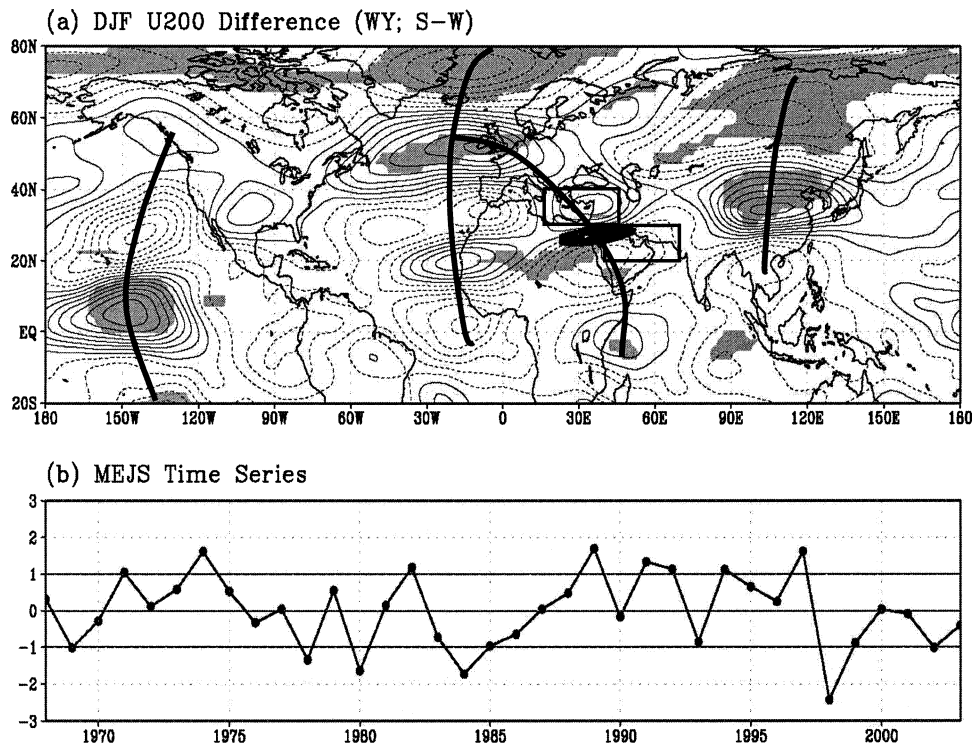FIG. 5. (a) Difference in the previous DJF U200 (m s^{-1}) between strong and weak JJA ASM (see Fig. 2). The thick lines mark the circulation features associated with different phenomena (e.g., ENSO, AO or NAO, and jet streams). The darkly shaded portion near Egypt, between the two boxes, indicates the climatological location of the Middle East jet stream. (b) Time series of the MEJS computed as the difference in DJF U200 between the southern (20°–30°N, 40°–70°E) and northern (30°–40°N, 15°–45°E) boxes shown in Fig. 5a (the former minus the latter). In Fig. 5a, the contour intervals are 1 m s^{-1} and values exceeding significantly the 90% confidence level are shaded. In Fig. 5b, the DJF of 1970/71 is labeled as 1970.

the extratropical North Pacific. Clearly, these features appearing over East Asia and the western Pacific are closely related to the variability of the East Asian jet stream (Yang et al. 2002), and thus implies a relationship between the ASM and this jet stream.

Although we will explore more about the previously discussed features by addressing the relationships among ASM, ENSO, and others, this study focuses on another outstanding feature. It can be seen from Fig. 5a that there exists a clear pattern over the eastern Atlantic and the western European–African region. This pattern represents a wave train that seems to be associated with the AO and the NAO (see Fig. 12 later). More interestingly, another wave train appears to the east and southeast of the earlier-mentioned pattern, extending from western Europe, the Mediterranean Sea, and the Middle East, to the western Arabian Sea. It looks like a subset of the AO- and NAO-related pattern. However, the key characteristic of this wave train is the southeast–northwest shift of the Middle East jet stream (MEJS), which is located climatologically over northern Egypt and Saudi Arabia, as highlighted in Fig. 5a (see the heavily shaded area in the figure). To measure the variability of the MEJS, we define an index from the difference in area-averaged U200 between the southern

(20°–30°N, 40°–70°E) and northern (30°–40°N, 15°–45°E) boxes as shown in Fig. 5a. Positive values of this index (see Fig. 5b) represent intensification and southeastward shift of the MEJS, and vice versa.

The relationship between the MEJS and the ASM revealed in Fig. 5a provides an important benchmark to pinpoint the antecedent signals identified by Webster and Yang (1992) and the physical processes from the signals to the monsoon. We claim that the variability of the MEJS is the key feature of these antecedent signals in the subtropical westerlies. Such an assertion may be rationalized for several reasons. First of all, as shown in Fig. 5a, the change in the upper-tropospheric westerlies (the monsoon's antecedent signals) is closely related to the change in the jet stream, which is significantly correlated to the Asian summer monsoon ($R = -0.46$; see Table 1). Second, compared to other larger-scale features like AO, which is also linked to the ASM, the change in the local jet stream enables a clearer physical explanation of the linkage between the signals and the monsoon. Third, the jet stream, which is located over the upstream region of the Tibetan Plateau and the ASM, favors the occurrence of many anomalies in surface conditions and maintains these anomalies that cause changes in the following monsoon. The

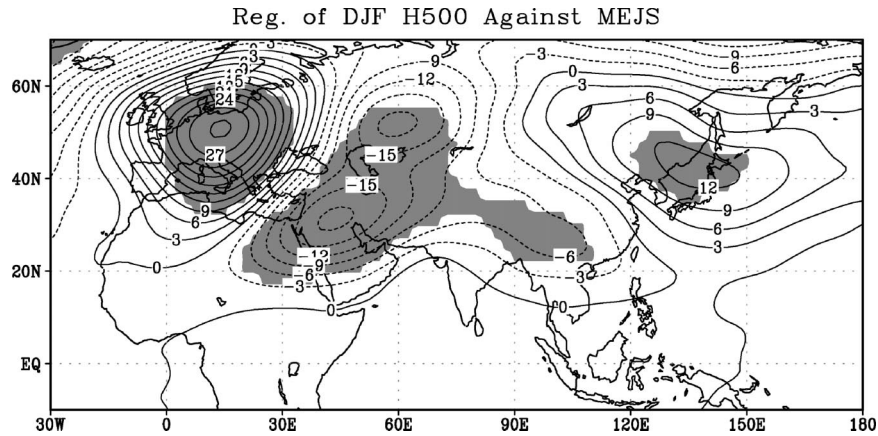Reg. of DJF H500 Against MEJS

FIG. 6. Regression of DJF 500-mb geopotential height against the MEJS index (see Fig. 5b). Units are meters. Areas in which the correlation exceeds significantly the 95% confidence level are shaded.

latter two points will be further ascertained in the next section.

4. Physical processes associated with the antecedent signals and the monsoon

The regression of DJF geopotential height at 500-mb (H500) against the MEJS is shown in Fig. 6. When the MEJS intensifies and shifts southeastward, a large-scale decrease in H500 occurs in Asia with an anomalous trough formed from western Russia to the Middle East, and to the west of the Tibetan Plateau. On the other hand, the geopotential height increases significantly over western Europe and northwestern Africa. This anomalous atmospheric pattern favors frequent southeastward intrusions of the cold air from central eastern Europe to the Middle East and southwestern Asia. Figure 6 also shows an anomalous high over the Sea of Japan, implying that the East Asian jet stream becomes weaker when the MEJS intensifies. This feature is consistent with that displayed in Fig. 5a, which shows that the East Asian jet stream becomes stronger when the MEJS weakens and shifts northwestward.

It is reasonable to anticipate that the robust anomalous atmospheric pattern in Fig. 6 is accompanied by corresponding changes in the temperature field. It can be seen from Fig. 7a, which shows the regression of DJF GTS T_s against the MEJS, that a strong MEJS is associated with a decrease in surface temperature in subtropical and tropical Asia. The cooling also extends to the central eastern North Africa and the eastern Mediterranean Sea. Associated with this feature is an increase in surface temperature in Europe and the higher latitudes of Asia. These MEJS-related changes shown in GTS T_s are further confirmed by an analysis of the GISS surface temperature (Fig. 7b). The latter, also providing information over the oceans and for longer period, shows relatively smoother features.

Figure 8a shows the difference in snow extent between the strong and weak MEJS winters. Positive values indicate the numbers of weeks that snow cover is more extensive during the strong MEJS winters than during the weak MEJS winters. Correspondingly, negative values indicate relatively less extensive snow during the strong jet stream winters. When the jet stream is strong, more extensive snow appears in eastern Europe, western Asia, and the east of the Mediterranean Sea. While mixed signals appear in central Asia, less extensive snow occurs in western Europe. It should be noted that presented in Fig. 8a is only the snow extent information. A sufficiently long record of continental-scale snow depth (or equivalent water) is unavailable for our analysis. Thus, we show in Fig. 8b the corresponding difference pattern for winter precipitation, which includes the snow amount information. Precipitation is also an important factor in determining the content of soil moisture, whose memory explains the persistence in the features associated with premonsoon atmospheric circulation and the development of ASM (e.g., Yang et al. 1996; Lau and Bua 1998; Yang and Lau 1998). Unfortunately, long-term, continental-scale records of soil moisture, which could be used to independently verify the relationship, are also not available at present. Figure 8b reveals that, when the MEJS is strong, there is more precipitation in the broad region encompassing subtropical–extratropical Asia and the Middle East, and less precipitation over western and northern Europe. Therefore, the various, independent data fields of surface temperature, snow cover, and precipitation shown in Figs. 7 and 8 exhibit consistent features associated with the variability of MEJS.

We also analyze the MEJS-related changes in the three-dimensional stationary wave activity flux (Plumb 1985; Yang and Gutowski 1994), which is more revealing and less misleading for analyzing wave behavior compared to energetic arguments, and higher-frequency atmospheric eddies (<10 days and 10–90 days, respectively). Results indicate that, when the MEJS intensifies
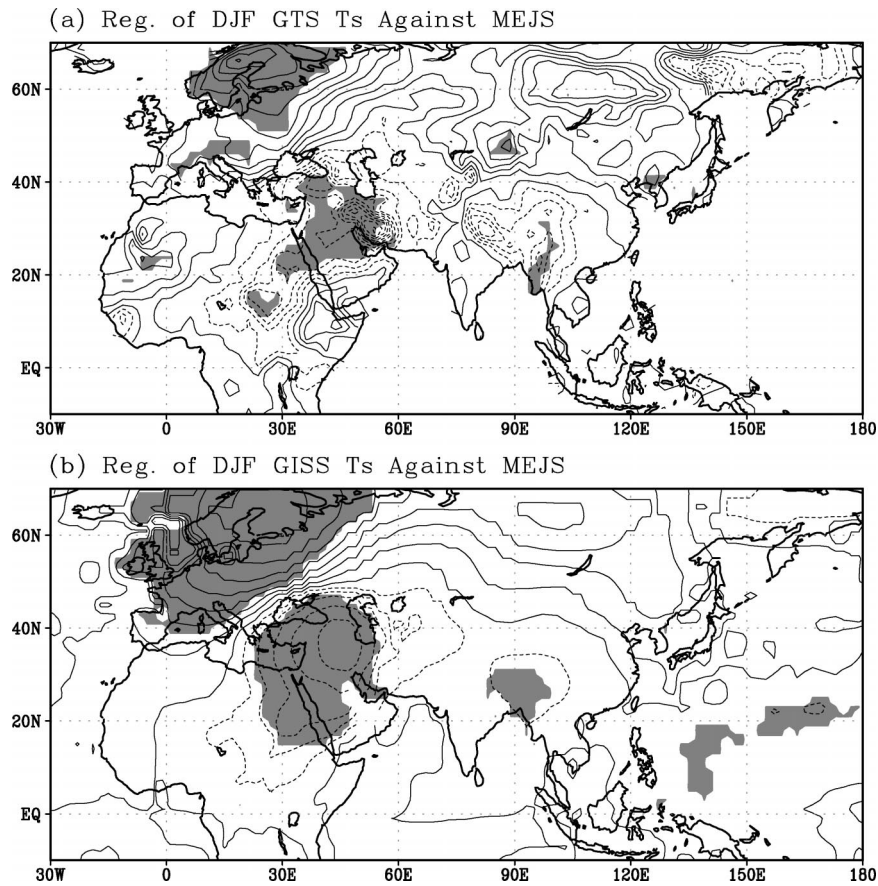
FIG. 7. Patterns of regression of (a) DJF GTS T_s and (b) DJF GISS T_s against the MEJS index (see Fig. 5b). Areas in which the correlation exceeds significantly the 95% confidence level are shaded.

and shifts southeastward, both stationary wave activity and eddy activity increase clearly in the southern Europe, Middle East, and southwestern Asia sectors (figures not shown). These changes are partially associated with synoptic features such as cold waves, which intrude into the regions more frequently under the favorable anomalous atmospheric conditions (see Fig. 6). Here, we emphasize the importance of the Tibetan Plateau, which affects the subtropical westerlies and tropical monsoon significantly (e.g., Bolin 1950; Murakami 1987; Li and Yanai 1996). The interaction between the Tibetan Plateau (e.g., its blocking effect) and the upstream MEJS to the west of the plateau leads to frequent occurrence of synoptic activities and acts to maintain the anomalies of surface temperature (Fig. 7) and atmospheric circulation (Fig. 6). This discussion is in agreement with the argument of Banerjee et al. (1978) and Mooley et al. (1986) about the relationship between the cold-season westerly activities and the Indian summer monsoon.

Next, we examine features of the land surface and the troposphere in MAM that are associated with the changes in MEJS, with a focus on the persistence of climate signals from winter to spring. Figure 9 reveals the relationships between DJF MEJS and the surface temperatures of following MAM. The regression maps show that, when the MEJS is strong, a large-scale cooling follows in Asia and Africa, between 10° and 40°N. In the meantime, a warming appears from the higher latitudes. The cooling and warming patterns are similar between Figs. 9a and 9b, where GTS and GISS T_s data are used, respectively. Importantly, a strong persistence in temperature anomalies emerges from DJF (Fig. 7) to MAM (Fig. 9) in subtropical Asia and the Middle East. The changes in snow and precipitation (see Fig. 8), and probably those in soil moisture (resulting from the changes in snow and precipitation) should play an important role in maintaining these temperature anomalies.

The persistent cooling in subtropical Asia and the Middle East, shown in Figs. 7 and 9, should be closely related to the signals in the overlying atmosphere. It can be seen from Fig. 10, a regression map of MAM geopotential height at 200 mb (H200) against the DJF MEJS, that the H200 decreases significantly over the cooling area associated with strong MEJS. A remarkable feature of Fig. 10 is the negative band between 15° and

(a) Difference in Snow Cover (MEJS; S−W)

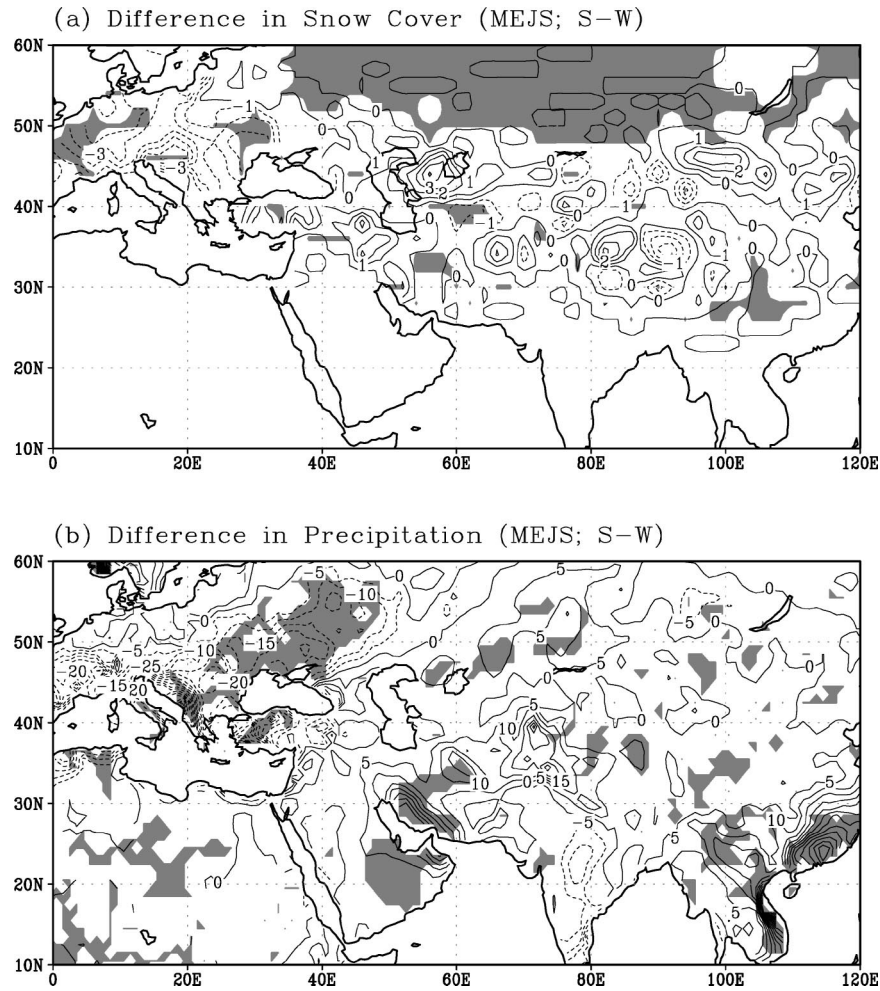(b) Difference in Precipitation (MEJS; S−W)

FIG. 8. (a) Difference in DJF snow extent between strong and weak MEJS. Shown is the difference in the number of weeks with snow between the strong MEJS winters and weak MEJS winters. (b) Difference in DJF precipitation (mm month^{-1}) between strong and weak MEJS. Winters of strong MEJS include 1971/72, 1974/75, 1982/83, 1989/90, 1991/92, 1992/93, 1994/95, and 1997/98; and those of weak MEJS include 1969/70, 1978/79, 1980/81, 1984/85, 1985/86, 1998/99, and 2002/03. Fewer samples are used for the snow data, which are available for the period starting 1972. Units are °C. Values exceeding significantly the 95% confidence level are shaded.

40°N and the generally positive band to the north. However, we should focus on the negative center over Iran, Afghanistan, Pakistan, India, and China, as highlighted by the box in the figure. This center of decreased H200 is of particular interest because it appears over the location of the South Asian high, which begins to dominate the region in late spring and early summer and plays a vital role in affecting the development of the ASM. Although Figs. 9 and 10 show consistently the features of negative anomalies of surface temperature and upper-tropospheric geopotential height over the Middle East and subtropical Asia, we should not claim a cause-and-effect relationship between the two fields, both of which have been linked to the variability of MEJS.

The importance of the thermal and dynamical state of the Tibetan Plateau for the development of the overlying atmospheric anomalies and the following summer monsoon has been demonstrated convincingly by many previous studies (e.g., Gadgil 1977; Luo and Yanai 1984; He et al. 1987; Yanai et al. 1992; Ueda and Yasunari 1998) and is thus not discussed here. Suffice it to say that the decreased H200 over South Asia, meaning a late establishment of the South Asian high, apparently delays the atmospheric transition from winter to summer conditions. In particular, the MAM H200 within the box of Fig. 10 is strongly correlated with both the antecedent DJF MEJS ($R = -0.43$) and the following summer monsoon ($R = 0.61$). That is, the spring anomalies over South Asia are closely associated with changes of the previous winter subtropical westerlies and the following summer monsoon. Indeed, the summer monsoon is
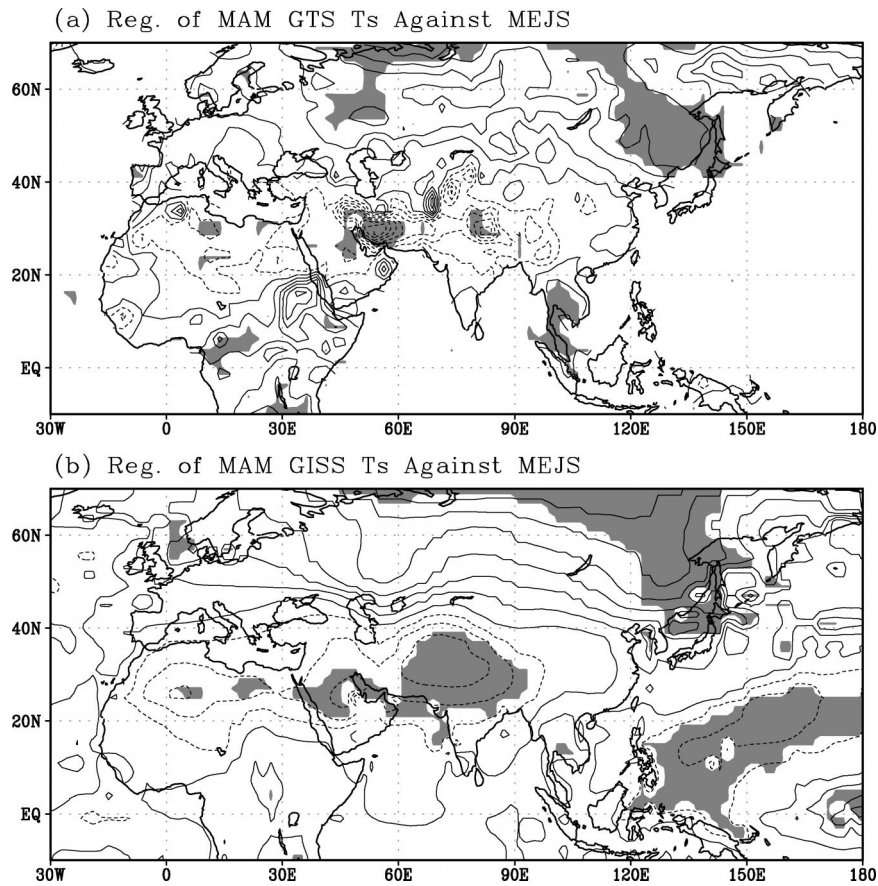
(a) Reg. of MAM GTS Ts Against MEJS

(b) Reg. of MAM GISS Ts Against MEJS

FIG. 9. Patterns of regression of (a) MAM GTS T_s and (b) MAM GISS T_s against the antecedent DJF MEJS index. Units are °C. Areas in which the correlation exceeds significantly the 90% confidence level are shaded.

strongly correlated with the precursory DJF MEJS with a coefficient of -0.46, while the correlation between the monsoon and the previous DJF Niño-3 SST is much weaker ($R = -0.23$). These results are summarized in Table 1 (especially column 3), which clearly shows the

practical significance of the antecedent signals for ASM prediction.

We further demonstrate the relationships among DJF MEJS, MAM H200, and JJA monsoon by showing the histograms of MEJS and H200 relative to the intensity
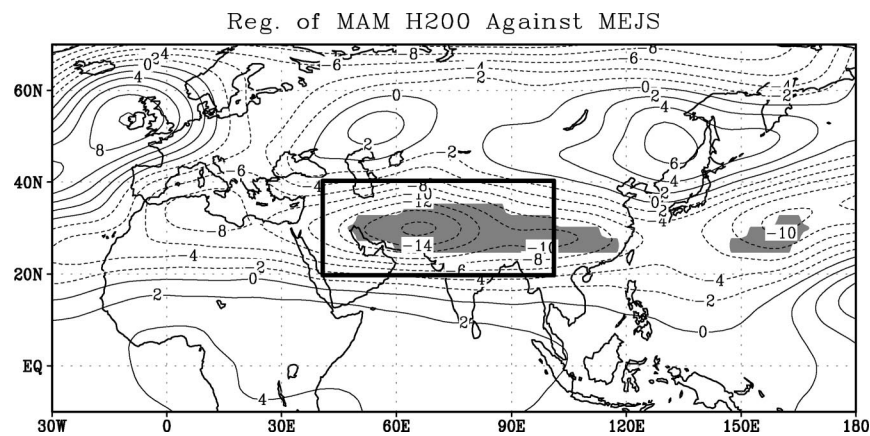
Reg. of MAM H200 Against MEJS

FIG. 10. Regression of MAM 200-mb geopotential height against the antecedent DJF MEJS index. The box highlights the domain of 20°–40°N, 40°–100°E. Units are meters. Areas in which the correlation exceeds significantly the 95% confidence level are shaded.
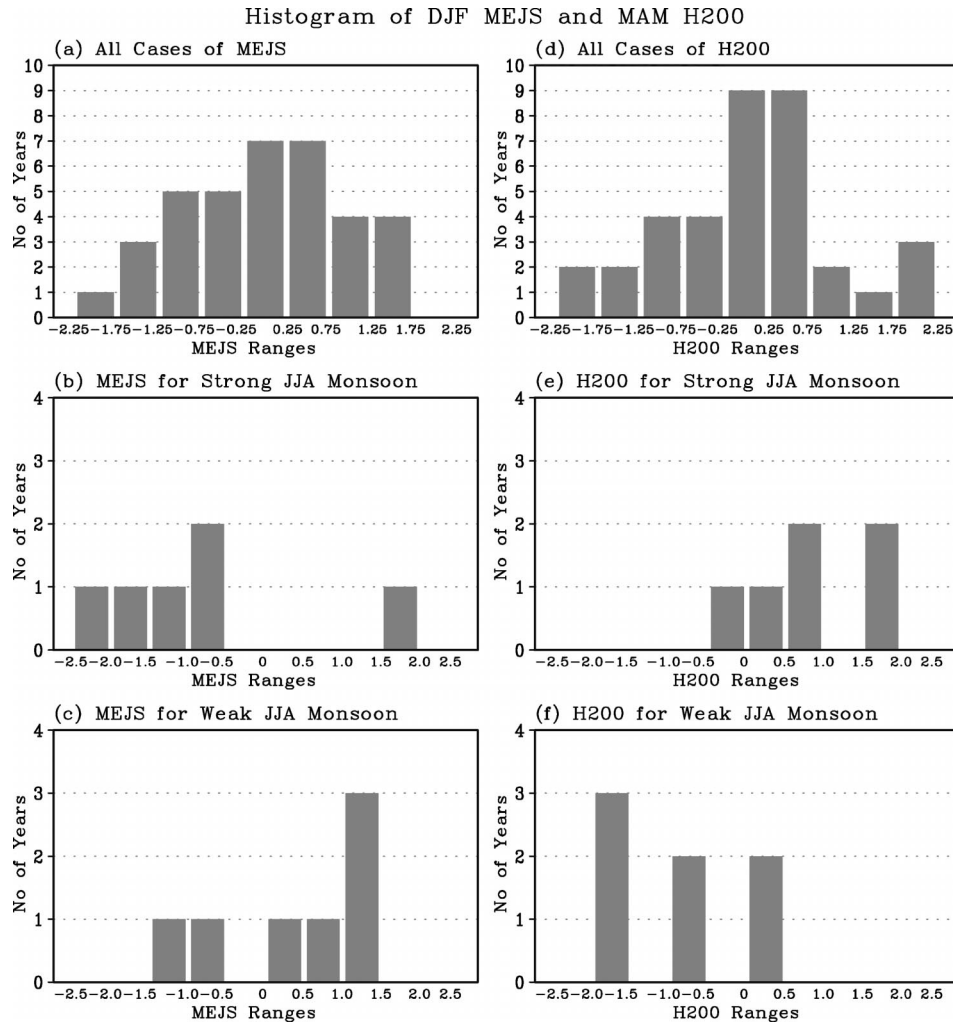
Histogram of DJF MEJS and MAM H200

FIG. 11. Histogram of DJF MEJS for (a) all years and separately for (b) strong and (c) weak summer monsoon years. (d)–(f) The same as in (a)–(c) except for MAM H200 (see the box in Fig. 10). Shown in *x* coordinate are normalized values.

of the monsoon. Figure 11a shows a pattern like standard distribution function for MEJS. Among the 6 yr of strong monsoon, weak jet stream occurs in 5 yr (Fig. 11b). Also, the jet stream is stronger than normal in 5 out of the 7 yr of weaker monsoon (Fig. 11c). In spite of the small number of samples, a clear separation of MEJF is seen between the strong and weak monsoon cases. Similar features can also be found between MAM

H200 and JJA monsoon (Figs. 11d–f). Namely, the MAM H200 increases in 5 of the 6 strong monsoon years and decreases in 5 of 7 weak monsoon years. The H200 anomalies that change oppositely to this tendency appear only in the very weak ranges.

It may also be interesting to note that, although the MAM H200 over South Asia is significantly correlated to the DJF MEJS, it has no apparent relationship with the previous ENSO conditions. Especially, the coefficients of its correlation with the Niño-3 SST of the previous DJF and the concurrent MAM are 0.12 and -0.14, respectively (see Table 1, column 2).

Compared to the wintertime simultaneous relationship between MEJS and surface temperature, the significance of correlation between the winter MEJS and the spring temperature decreases (see Figs. 7 and 9). While such a reduction in correlation significance seems natural, we have not explained how tropical factors play a role in the persistence of the temperature signals from

TABLE 1. Correlation between the JJA Asian summer monsoon (measured by the WY index) and antecedent climate signals. The bold italic numbers indicate the correlation exceeding significantly the 99% confidence level.

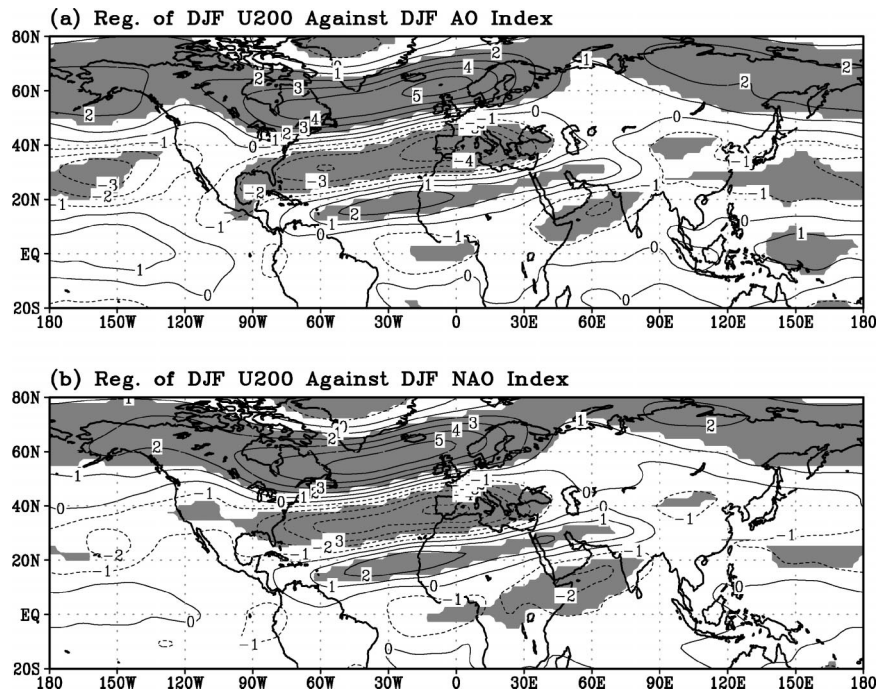|	MAM H200	JJA Monsoon
DJF Niño-3 SST	0.12	-0.23
DJF MEJS	*−0.43*	*−0.46*
MAM Niño-3 SST	-0.14	*−0.46*
MAM H200	1.00	*0.61*

FIG. 12. Regression of DJF U200 against (a) DJF AO and (b) DJF NAO. Units are m s^{-1}. Areas in which the correlation exceeds significantly the 95% confidence level are shaded.

winter to spring when the extratropical (westerly) systems become less vigorous. The enhanced signal over the tropical western Pacific shown in Fig. 9 implies the increasing importance of tropical heating, which is central to the mechanism for explaining the TBO (Meehl 1997; Ogasawara et al. 1999; Meehl and Arblaster 2002a).

5. Large-scale teleconnection of monsoon's antecedent signals

After depicting the physical processes linking the precursory signals to the Asian summer monsoon in the previous section, we now inquire how these antecedent changes, especially those in the MEJS, are related to other large-scale climate phenomena in winter. Compared to the East Asian jet stream, the MEJS and its seasonal-to-interannual variability have received much less attention and many related features remain unknown. However, it is assumed that, although the variability of MEJS is governed largely by the internal dynamics of the atmosphere, external forcing also plays a certain role, as is the case for the East Asian jet stream (see Yang et al. 2002 and references therein). A detailed analysis of the physical mechanisms for the variability of MEJS is not easily available and beyond the scope of this study. However, it is believed that a careful analysis of the relationship between MEJS and slowly varying surface forcing or large-scale atmospheric patterns is helpful for improving our understanding of the var-

iability of the jet stream and its relationship with the Asian monsoon.

Figure 5a, though focused on ASM-related features, has already hinted a connection of MEJS with AO or NAO, and also possibly with ENSO and the East Asian jet stream. Here we further investigate these features by first comparing Fig. 5a with the regression patterns of U200 against AO and NAO (http://www.cpc.noaa.gov/products/precip/CWlink/all_index.html). As seen from Fig. 12a, the regression against AO exhibits a wave train–like pattern, which initiates from Greenland and becomes two branches west of the Mediterranean Sea, one extending southward along the western Africa coast and the other reaching southeastward to the Arabian Sea. A consistent feature also appears in Fig. 12b, associated with the NAO. This is not surprising because of the generally strong correlation between AO and NAO. It is not difficult to see that these dominant features are similar to those previously found in Fig. 5a. Therefore, the MEJS, AO, and NAO are all associated with similar features of U200 over the regions of the eastern Atlantic, Europe, Africa, and western Asia including the Middle East. The MEJS intensifies during the positive phase of AO and NAO, and the correlation of MEJS with AO ($R = 0.36$) and NAO ($R = 0.33$) significantly exceeds the 95% confidence level.

We also examine the simultaneous relations of MEJS with the Pacific decadal oscillation (PDO) and the East Asian jet stream. There exists only weak evidence that MEJS becomes stronger (weaker) during the negative
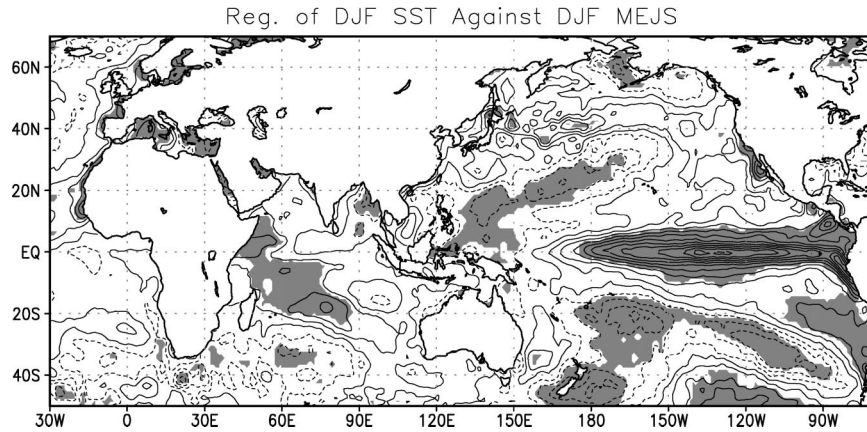
Reg. of DJF SST Against DJF MEJS

FIG. 13. Regression of DJF SST against the MEJS index. Units are °C. Areas in which the correlation exceeds significantly the 90% confidence level are shaded.

(positive) phase of PDO, for which longer data records are needed. However, the MEJS is more strongly and negatively correlated with the East Asian jet stream ($R = -0.4$). Here, we use the index of Yang et al. (2002) to measure the East Asian jet stream, which is the DJF U200 averaged over 30°–35°N, 130°–160°E.

Figure 13 shows the simultaneous relationship between MEJS and the DJF SST spatial pattern. During the winters when the MEJS is strong, a significant warming appears in the tropical central eastern Pacific. Thus, the figure shows a feature that bears a resemblance to that associated with ENSO and suggests a relationship between MEJS and ENSO. In fact, the coefficient of simultaneous correlation between MEJS and Niño-3 SST is 0.31, which is only moderate compared to the correlation of MEJS with AO or NAO. It is also interesting to note that, associated with strong MEJS, cooling occurs in the Tropics and warming in the extratropics of the western Pacific. These SST changes are accompanied by a weaker East Asian jet stream (Yang et al. 2002), conforming the reserved relationship between this jet stream and MEJS shown in Figs. 5a, 6, and 12.

Figure 13 also reveals a MEJS-related warming, though relatively weaker, in the tropical Indian Ocean, which may not be necessarily linked to ENSO SST anomalies, at least not directly. Combining this feature with the cooling in the subtropical land area in the Middle East and Asia (see Figs. 7 and 9) indicates another important feature: the MEJS varies in association with changes in the meridional temperature gradient. To gain an insight into the relationship between MEJS and meridional temperature gradient, we plot in Fig. 14 the monthly values of MEJS (Fig. 14a) and meridional temperature gradient (Figs. 14b,c), respectively, with respect to strong and weak DJF MEJS. In the figure, the solid (dashed) lines measure the values of strong (weak) MEJS cases, and the thin and thick lines show the values of each year and the averages of all years (separately for strong and weak cases), respectively. For Fig. 14b, we use GISS T_s over a Southern Ocean domain (10°S–

20°N, 20°–80°E) and a northern land domain (20°–40°N, 20°–80°E). The values represent the differences in the surface temperature between the two domains (southern minus northern), for strong and weak MEJS cases. Similarly for Fig. 14c, we apply SST for the southern domain and GTS T_s for the northern domain. (Note that the GTS data are only available for land areas.)

Figure 14 shows that a stronger (weaker) MEJS in winter is preceded and accompanied by a larger (smaller) meridional temperature gradient in late fall and winter. Various, independent data fields (SST and GISS and GTS surface temperatures) are analyzed and presented to emphasize the consistency and robustness of the relationship between the MEJS and meridional temperature gradient. These features are in agreement with the result of Li and Yanai (1996) who depicted the onset and interannual variability of the Asian summer monsoon and their relationship with land–sea thermal contrast. They are also consistent with the context of TBO in which the importance of warming and cooling in the Indian Ocean is stressed (Meehl 1997; Chang and Li 2000; Meehl and Arblaster 2002a). It can also be seen that a stronger (weaker) MEJS is accompanied by a larger (smaller) temperature gradient in the following spring. This feature may result from the interaction between the atmosphere and the land surface processes. As shown before (Figs. 7 and 9), when the MEJS intensifies and shifts southeastward, surface temperature decreases and, as a result, the meridional gradient of temperature increases. Thus, if the meridional temperature gradient is one of the possibly many forcing functions of the MEJS, the change in the jet stream seems to reinforce the temperature forcing.

6. Summary and further discussion

a. Summary

In this study, we have examined the features of subtropical atmospheric and land surface processes that are
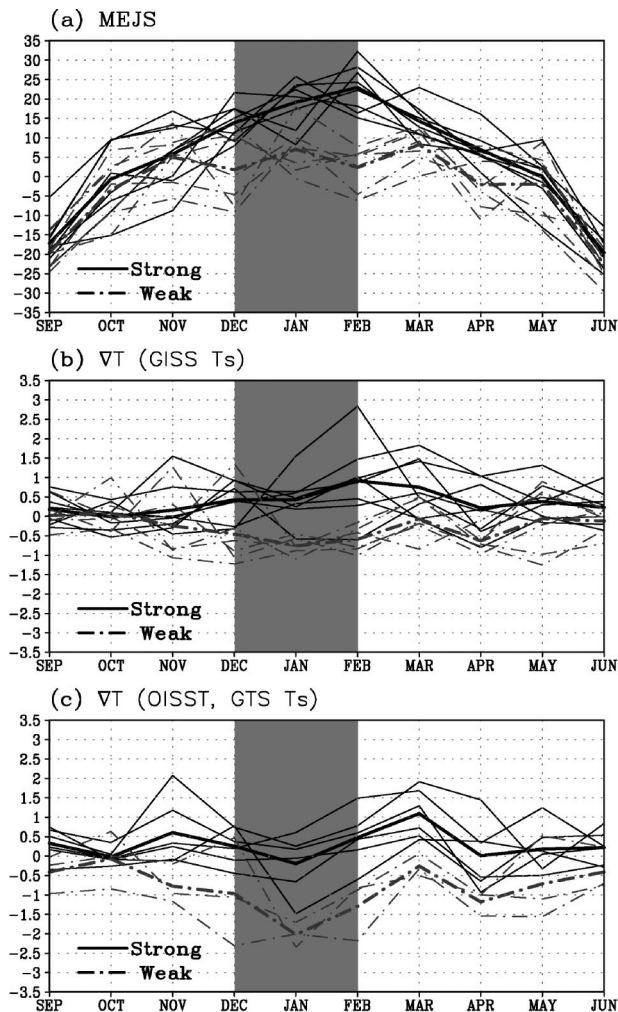
FIG. 14. (a) Composite (thick lines) and yearly (thin lines) values of monthly MEJS (m s^{-1}) for strong (solid lines) and weak (dashed lines) DJF MEJS. See Fig. 8 for the years of strong and weak MEJS. (b) Composite and yearly values of monthly GISS T_s gradient (°C) between a southern (10°S–20°N, 20°–80°E) and a northern (20°–40°N, 20°–80°E) domains, for strong and weak MEJS. (c) Same as in (b) but for SST (°C) in the southern domain and GTS T_s in the northern domain. (Fewer samples are used for the GTS T_s, which covers the period starting 1979.)

associated with the Asian summer monsoon. In particular, we have discussed several issues related to the antecedent signals of a large-scale monsoon in the upper-tropospheric westerlies over subtropical Asia previously identified by Webster and Yang (1992). We have revisited the antecedent signals using updated observations, depicted their detailed structure, and investigated the physical process from the signals to the monsoon. We have also explored the teleconnection of the signals to large-scale climate phenomena and emphasized the importance of the upstream location of the signals relative to the Tibetan Plateau and the monsoon.

A salient feature before a strong (weak) summer monsoon is that the upper-tropospheric westerlies over sub-

tropical Asia are weaker (stronger) than normal during the previous winter and spring. In this study, we have demonstrated that the variability of the Middle East jet stream represents the key feature of the monsoon's antecedent signals. To explore this feature, we have constructed an index to measure the changes of the jet stream, including its northwest–southeast shift. The variations of this jet stream are linked to the Arctic Oscillation, the North Atlantic Oscillation, El Niño–Southern Oscillation, and the East Asian jet stream. The intensification and southeastward shift of the MEJS favor frequent intrusions of the cold air from eastern Europe into the Middle East and southwestern Asia. As a result, in subtropical Asia, snow and precipitation increase, the ground wetness increases, and surface temperature decreases. A strengthening MEJS is also accompanied by increases in both stationary wave activity flux and higher-frequency eddy activity over southern Europe, the Middle East, and southwestern Asia. The Tibetan Plateau tends to block these westerly activities and increase the persistence of the negative temperature anomalies, which in turn explain the enduring atmospheric signals from winter to spring seasons.

A strong link is found between the persistent low temperature anomalies and the decrease in geopotential height over South Asia, near the Tibetan Plateau, in spring. The latter means a late establishment of the South Asian high and thus a delay in the atmospheric transition from the winter to summer conditions. All of these features hamper the development of a strong monsoon during the following summer. The reverse scenario of a weaker MEJS and a stronger Asian monsoon also holds.

b. Further discussion

Although we have provided a clear physical picture about the association of the AMS with extratropical antecedent signals and other climate phenomena especially the Middle East jet stream, whose variability has rarely been documented, we have not claimed a cause-and-effect relationship between the signals and the monsoon. Even if such a relationship exists, the variability of the monsoon is also governed by many other factors and caution should thus be taken when the precursory signals are applied to monsoon prediction. Yet, this study has yielded several results that are helpful for monsoon prediction. As summarized in Table 1, the ASM is more significantly correlated to the previous DJF MEJS ($R = -0.46$) than to DJF Niño-3 SST ($R = -0.23$). Also, the MAM H200 over Tibetan Plateau, which is strongly associated with ASM, is more significantly correlated to the DJF MEJS ($R = -0.43$) than to DJF Niño-3 SST ($R = 0.12$) and MAM Niño-3 SST ($R = -0.14$).

For the link between the antecedent extratropical signals and ASM, this study has demonstrated several features that are similar to those previously applied to explain the mechanism for TBO via tropical–extratropical
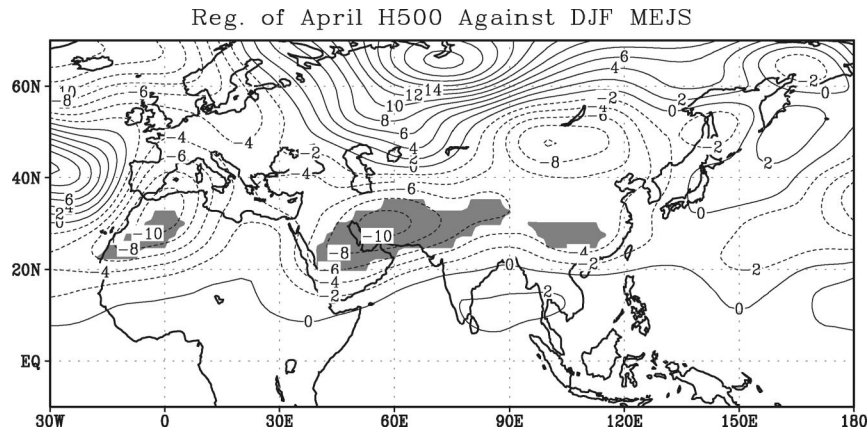
Reg. of April H500 Against DJF MEJS

FIG. 15. Regression of Apr H500 against the antecedent DJF MEJS index. Units are meters. Areas in which the correlation exceeds significantly the 95% confidence level are shaded.

interactions (e.g., Meehl 1997; Ogasawara et al. 1999; Meehl and Arblaster 2002a,b). For example, before a strong summer monsoon over South Asia, an anomalous ridge and less snow and warmer conditions appear over Eurasia in winter. However, in this TBO mechanism, the previously mentioned wintertime signals and their persistence through MAM are related to the variability of tropical SST and to the memories in the SST and associated thermocline conditions. That is, the extra-tropical signals over Eurasia are mainly treated as a Rossby wave response to tropical heating and, according to Ogasawara et al. (1999), the major tropical forcing is the convection anomalies over Indonesia and northern Australia. Within the context of TBO, Yasunari and Seki (1992) also linked the regional Indian monsoon to NAO. However, the authors claimed that the NAO varies independently from ENSO, which should be demonstrated by further evidence.

In this study, while we stress the influence of extratropical factors on ASM, we do not de-emphasize the importance of ENSO as an influential factor or a precursor of the monsoon. In fact, we have discussed in section 5 the association of ENSO with the subtropical signals and its possible role in the physical process from the signals to the monsoon. This discussion is consistent with that of Yang and Lau (1998) who described such a role as the indirect impact of ENSO on the monsoon. However, it is difficult to assess what portion of the signals and their contributions to monsoon variability can be explained by ENSO. This is even a very difficult task for studies in which carefully designed experiments are carried out using atmospheric general circulation models, as in the work conducted by Yang and Lau. Nevertheless, this study indicates that the MEJS, the key component of the antecedent signals of ASM, is more strongly related to the East Asian jet stream, AO, and NAO than to ENSO in winter.

Finally, we address the possible connection between the midtropospheric ridge over the tropical India peninsula (a good indicator for the regional Indian monsoon rainfall) and the extratropical signals discussed in this study (precursors of the large-scale Asian monsoon circulation). This issue is also related to the previous inquiries about the relationship of the large-scale Asian monsoon to the Indian monsoon and other components (Webster and Yang 1992; Goswami et al. 1999; Wang and Fan 1999; Lau et al. 2000). Figure 15 shows the regression of April H500 against DJF MEJS. It indicates that following a strong MEJS, which is accompanied by decreased surface temperature and geopotential height (see Figs. 9 and 10) and weakened ASM, the H500 decreases over Iran, Pakistan, and northern India but increases over southern India and the Bay of Bengal, meaning a southward shift of the midtropospheric ridge. This feature is indeed the characteristic feature of the relationship in which a southward shift of the ridge is followed by a late onset and weaker-than-normal Indian summer monsoon (see Shukla and Mooley 1987). The figure also implies an in-phase variability of the regional Indian monsoon and the large-scale Asian monsoon measured by the WY index. Indeed, some moderate relationships have been found in the correlation of the Indian monsoon to the DJF MEJS and to the MAM H200 over the Tibetan Plateau. These relationships, though they are not extremely strong, provide support for the results obtained in this study. However, it should be pointed out that the relatively small-scale ridge should be distinguished from the much larger scale antecedent signals examined in this study. Furthermore, it may not be appropriate to apply the midtropospheric ridge to the prediction of broad-scale monsoon circulation although it is linked to the regional Indian monsoon and the extratropical signals.

REFERENCES

Annaamalai, H., J. M. Slingo, K. R. Sperber, and K. Hodges, 1999: The mean evolution and variability of the Asian summer monsoon: Comparison of ECMWF and NCEP–NCAR reanalyses. *Mon. Wea. Rev.,* **127,** 1157–1186.

Bamzai, A. S., and J. Shukla, 1999: Relation between Eurasian snow cover, snow depth, and the Indian summer monsoon: An observational study. *J. Climate,* **12,** 3117–3132.

Banerjee, A. K., P. N. Sen, and C. R. V. Raman, 1978: On foreshadowing southwest monsoon rainfall over India with midtropospheric circulation anomaly of April. *Indian J. Meteor. Geophys.,* **29,** 425–431.

Barnett, T. P., L. Dumenil, U. Schlese, E. Roecker, and M. Latif, 1989: The effect of Eurasian snow cover on regional and global climate variations. *J. Atmos. Sci.,* **46,** 661–685.

Blanford, H. F., 1884: On the connexion of Himalayan snowfall and seasons of drought in India. *Proc. Roy. Soc. London,* **37,** 3–22.

Bolin, B., 1950: On the influence of the earth's orography on the general character of the westerlies. *Tellus,* **2,** 184–196.

Chang, C.-P., and T. Li, 2000: A theory for the tropospheric biennial oscillation. *J. Atmos. Sci.,* **57,** 2209–2224.

——, P. Harr, and J. Ju, 2001: Possible roles of Atlantic circulations on the weakening Indian monsoon rainfall–ENSO relationship. *J. Climate,* **14,** 2376–2380.

Dugam, S. S., S. B. Kakade, and R. K. Verma, 1997: Interannual and long term variability in the North Atlantic Oscillation and Indian summer monsoon rainfall. *Theor. Appl. Climatol.,* **58,** 21–29.

Gadgil, S., 1977: Orographic effects on the Southwest monsoon: A review. *Pure Appl. Geophys.,* **115,** 1413–1430.

Gong, D.-Y., and C.-H. Ho, 2003: Arctic Oscillation signals in the East Asian summer monsoon. *J. Geophys. Res.,* **108,** 4066, doi:10.1029/2002JD002193.

Goswami, B. N., V. Krishnamurthy, and H. Annamalai, 1999: A broad scale circulation index for the interannual variability of the Indian summer monsoon. *Quart. J. Roy. Meteor. Soc.,* **125,** 611–633.

Hahn, D. G., and J. Shukla, 1976: An apparent relationship between Eurasian snow cover and Indian monsoon rainfall. *J. Atmos. Sci.,* **33,** 2461–2462.

Hansen, J., R. Ruedy, J. Glascoe, and M. Sato, 1999: GISS analysis of surface temperature change. *J. Geophys. Res.,* **104,** 30 997–31 022.

He, H., J. W. McGinnis, Z. Song, and M. Yanai, 1987: Onset of the Asian monsoon in 1979 and the effect of the Tibetan Plateau. *Mon. Wea. Rev.,* **115,** 1966–1995.

Ju, J., and J. M. Slingo, 1995: The Asian Summer Monsoon and ENSO. *Quart. J. Roy. Meteor. Soc.,* **121,** 1133–1168.

Kalnay, E., and Coauthors, 1996: The NCEP/NCAR 40-Year Reanalysis Project. *Bull. Amer. Meteor. Soc.,* **77,** 437–471.

Kawamura, R., 1998: A possible mechanism of the Asian summer monsoon–ENSO coupling. *J. Meteor. Soc. Japan,* **76,** 1009–1027.

Lau, K. M., and W. R. Bua, 1998: Mechanism of monsoon–Southern Oscillation coupling: Insights from GCM experiments. *Climate Dyn.,* **14,** 759–779.

——, and M. J. Nath, 2000: Impact of ENSO on the variability of the Asian–Australian monsoons as simulated in GCM experiments. *J. Climate,* **13,** 4287–4309.

——, K.-M. Kim, and S. Yang, 2000: Dynamical and boundary forcing characteristics of regional components of the Asian summer monsoon. *J. Climate,* **13,** 2461–2482.

Li, C., and M. Yanai, 1996: The onset and interannual variability of the Asian summer monsoon in relation to land–sea thermal contrast. *J. Climate,* **9,** 358–375.

LinHo, and B. Wang, 2002: The time–space structure of the Asian–Pacific summer monsoon: A fast annual cycle view. *J. Climate,* **15,** 2001–2019.

Luo, H., and M. Yanai, 1984: The large-scale circulation and heat sources over the Tibetan Plateau and surrounding areas during the early summer of 1979. Part II: Heat and moisture budgets. *Mon. Wea. Rev.,* **112,** 966–989.

Meehl, G. A., 1987: The annual cycle and interannual variability in the tropical Indian and Pacific Ocean regions. *Mon. Wea. Rev.,* **115,** 27–50.

——, 1994: Influence of the land surface in the Asian summer monsoon: External conditions versus internal feedbacks. *J. Climate,* **7,** 1033–1049.

——, 1997: The South Asian monsoon and the tropospheric biennial oscillation. *J. Climate,* **10,** 1921–1943.

——, and J. M. Arblaster, 2002a: The tropospheric biennial oscillation and Asian–Australian monsoon rainfall. *J. Climate,* **15,** 722–744.

——, and ——, 2002b: Indian monsoon GCM sensitivity experiments testing tropospheric biennial oscillation transition conditions. *J. Climate,* **15,** 923–944.

Miyakoda, K., A. Navarra, and M. N. Ward, 1999: Tropical-wide teleconnection and oscillation. II: The ENSO–monsoon system. *Quart. J. Roy. Meteor. Soc.,* **125,** 2937–2963.

——, J. L. Kinter, and S. Yang, 2003: The role of ENSO in the South Asian monsoon and pre-monsoon signals over the Tibetan Plateau. *J. Meteor. Soc. Japan,* **81,** 1015–1039.

Mooley, D. A., B. Parthasarathy, and G. B. Pant, 1986: Relationship between Indian summer monsoon rainfall and location of the ridge at the 500-mb level along 75°E. *J. Climate Appl. Meteor.,* **25,** 633–640.

Murakami, T., 1987: Effects of the Tibetan Plateau. *Monsoon Meteorology,* C.-P. Chang and T. N. Krishnamurti, Eds., Oxford University Press, 235–270.

——, and Y.-H. Ding, 1982: Wind and temperature changes over Eurasia during the early summer of 1979. *J. Meteor. Soc. Japan,* **60,** 183–196.

——, L.-X. Chen, and A. Xie, 1986: Relationship among seasonal cycles, low-frequency oscillations, and transient disturbances as revealed from outgoing longwave radiation data. *Mon. Wea. Rev.,* **114,** 1456–1465.

Navarra, A., M. N. Ward, and K. Miyakoda, 1999: Tropical-wide teleconnection and oscillation. I: Teleconnection indices and type I/type II states. *Quart. J. Roy. Meteor. Soc.,* **125,** 2909–2935.

New, M. G., M. Hulme, and P. D. Jones, 1999: Representing twentieth-century space–time climate variability. Part I: Development of a 1961–90 mean monthly terrestrial climatology. *J. Climate,* **12,** 829–856.

——, ——, and ——, 2000: Representing twentieth-century space–time climate variability. Part II: Development of 1901–1996 monthly grids of terrestrial surface climate. *J. Climate,* **13,** 2217–2238.

Normand, C., 1953: Monsoon seasonal forecasting. *Quart. J. Roy. Meteor. Soc.,* **79,** 463–473.

Ogasawara, N., A. Kitoh, T. Yasunari, and A. Noda, 1999: Tropospheric biennial oscillation of ENSO–monsoon system in the MRI coupled GCM. *J. Meteor. Soc. Japan,* **77,** 1247–1270.

Parthasarathy, B., K. Rupa Kumar, and A. A. Munot, 1991: Evidence of secular variations in Indian monsoon rainfall–circulation relationships. *J. Climate,* **4,** 927–938.

Peterson, T. C., and R. S. Vose, 1997: An overview of the Global Historical Climatology Network temperature database. *Bull. Amer. Meteor. Soc.,* **78,** 2837–2849.

Plumb, R. A., 1985: On the three-dimensional propagation of stationary waves. *J. Atmos. Sci.,* **42,** 217–229.

Ramaswamy, C., 1962: Breaks in the Indian summer monsoon as a phenomenon of interaction between the easterly and the subtropical westerly jet streams. *Tellus,* **14,** 337–349.

Rasmusson, E. M., and T. H. Carpenter, 1982: Variations in tropical sea surface temperature and surface wind fields associated with

the Southern Oscillation/El Nino. *Mon. Wea. Rev.,* **110,** 354–384.

Ropelewski, C. F., and M. S. Halpert, 1987: Global and regional scale precipitation patterns associated with the El Nino/Southern Oscillation. *Mon. Wea. Rev.,* **115,** 1606–1626.

Shen, X., M. Kimoto, and A. Sumi, 1998: Role of land surface processes associated with interannual variability of broad-scale Asian Summer Monsoon as simulated by the CCSR/NIES AGCM. *J. Meteor. Soc. Japan,* **76,** 217–236.

Shukla, J., and D. A. Paolino, 1983: The Southern Oscillation and long range forecasting of the summer monsoon rainfall over India. *Mon. Wea. Rev.,* **111,** 1830–1837.

——, and D. A. Mooley, 1987: Empirical prediction of the summer monsoon rainfall over India. *Mon. Wea. Rev.,* **115,** 695–703.

Slingo, J. M., and H. Annamalai, 2000: 1997: El Niño of the century and the response of the Indian monsoon. *Mon. Wea. Rev.,* **128,** 1778–1797.

Smith, T. M., and R. W. Reynolds, 2003: Extended reconstruction of global sea surface temperatures based on COADS data (1854–1997). *J. Climate,* **16,** 1495–1510.

Soman, M. K., and J. M. Slingo, 1997: Sensitivity of the Asian summer monsoon to aspects of the sea surface temperature anomalies in the tropical Pacific Ocean. *Quart. J. Roy. Meteor. Soc.,* **123,** 309–336.

Tao, S., and Q. Zhang, 1998: Response of the East Asian summer monsoon to ENSO events (in Chinese). *Sci. Atmos. Sinica,* **22,** 399–407.

Thapliyal, V., 1982: Stochastic dynamic model for long-range prediction of monsoon rainfall in Peninsular India. *Mausam,* **33,** 399–404.

Thomas, B., S. V. Kasture, and V. Satyan, 2000: Links between tropical SST anomalies and precursory signals associated with the interannual variability of Asian summer monsoon. *Meteor. Atmos. Phys.,* **75,** 39–49.

Ueda, H., and T. Yasunari, 1998: Role of warming over the Tibetan Plateau in early onset of the summer monsoon over the Bay of Bengal and the South China Sea. *J. Meteor. Soc. Japan,* **76,** 1–12.

Walker, G. T., 1923: Correlation in seasonal variations of weather VIII. *Mem. Indian Meteor. Dept.,* **24,** 75–131.

——, 1924: World Weather IX. *Mem. Indian Meteor. Dept.,* **24,** 275–332.

Wang, B., and Z. Fan, 1999: Choice of South Asian summer monsoon indices. *Bull. Amer. Meteor. Soc.,* **80,** 629–638.

——, and T. Li, 2004: *East Asian Monsoon and ENSO Interaction, East Asian Monsoon.* Series on Meteorology of East Asia, Vol. 2, World Scientific, in press.

——, R. Wu, and X. Fu, 2000: Pacific–East Asia teleconnection: How does ENSO affect East Asian climate? *J. Climate,* **13,** 1517–1536.

Webster, P. J., and S. Yang, 1992: Monsoon and ENSO: Selectively interactive systems. *Quart. J. Roy. Meteor. Soc.,* **118,** 877–926.

——, V. O. Magana, T. N. Palmer, J. Shukla, R. A. Tomas, M. Yanai, and T. Yasunari, 1998: Monsoons: Processes, predictability, and the prospects for prediction. *J. Geophys. Res.,* **103C,** 14 451–14 510.

Yanai, M., C. Li, and A. Song, 1992: Seasonal heating of the Tibetan Plateau and its effects of the evolution of the Asian summer monsoon. *J. Meteor. Soc. Japan,* **70,** 189–221.

Yang, S., and W. J. Gutowski, 1994: GCM simulations of the three-dimensional propagation of stationary waves. *J. Climate,* **7,** 414–433.

——, and K.-M. Lau, 1998: Influences of sea surface temperature and ground wetness on Asian summer monsoon. *J. Climate,* **11,** 3230–3246.

——, ——, and M. Sankar-Rao, 1996: Precursory signals associated with the interannual variability of the Asian summer monsoon. *J. Climate,* **9,** 949–964.

——, ——, and K.-M. Kim, 2002: Variations of the East Asian jet stream and Asian–Pacific–American winter climate anomalies. *J. Climate,* **15,** 306–325.

Yasunari, T., 1991: The monsoon year—A new concept of the climatic year in the Tropics. *Bull. Amer. Meteor. Soc.,* **72,** 1331–1338.

——, and Y. Seki, 1992: Role of the Asian monsoon on the interannual variability of the global coupled climate system. *J. Meteor. Soc. Japan,* **70,** 177–189.

Zeng, Q.-C., and B.-L. Zhang, 1998: On the seasonal variation of atmospheric general circulation and the monsoon. *Chin. J. Atmos. Sci.,* **22,** 211–220.

Zhang, R., A. Sumi, and M. Kimoto, 1996: Impact of El Niño on the East Asian monsoon: A diagnostic study of the '86/87 and '91/92 events. *J. Meteor. Soc. Japan,* **74,** 49–62.